Advances in Applied Mathematics and Mechanics
Adv. Appl. Math. Mech., Vol. **8**, No. 2, pp. 279-292

DOI: 10.4208/aamm.2013.m419
April 2016

Magnetohydrodynamic Natural Convection in a Rotating Enclosure

H. Saleh[1,*] and I. Hashim[2,3]

[1] *Solar Energy Research Institute, University Kebangsaan Malaysia, 43600 Bangi Selangor, Malaysia*
[2] *Pusat Pemodelan & Analisis Data, School of Mathematical Sciences, University Kebangsaan Malaysia, 43600 Bangi Selangor, Malaysia*
[3] *Research Institute, Center for Modeling & Computer Simulation (RI/CM&CS), King Fahd University of Petroleum & Minerals, Dhahran-31261, Saudi Arabia*

Received 4 December 2013; Accepted (in revised version) 18 March 2015

Abstract. Magnetohydrodynamic natural convection heat transfer in a rotating, differentially heated enclosure is studied numerically in this article. The governing equations are in velocity, pressure and temperature formulation and solved using the staggered grid arrangement together with MAC method. The governing parameters considered are the Hartmann number, $0 \leq Ha \leq 70$, the inclination angle of the magnetic field, $0^\circ \leq \theta \leq 90^\circ$, the Taylor number, $8.9 \times 10^4 \leq Ta \leq 1.1 \times 10^6$ and the centrifugal force is smaller than the Coriolis force and the both forces were kept below the buoyancy force. It is found that a sufficiently large Lorentz force neutralizes the effect of buoyancy, inertial and Coriolis forces. Horizontal or vertical direction of the magnetic field was most effective in reducing the global heat transfer.

AMS subject classifications: 65M06, 65M12, 76T05

Key words: Finite difference method, natural convection, MHD, rotating enclosure.

1 Introduction

Magnetohydrodynamics (MHD) deals with the dynamics of electrically conducting fluids, in which moving charge particles react to a magnetic field. MHD flow has been extensively studied due to its wide applications such as in controlling thermonuclear reactions in which the conducting fluid is a plasma confined by a magnetic field. The magnetohydrodynamic power generator is also an application of MHD flow. A magnetic field on thermally driven flow in a square enclosure was analytically studied by [6]. [18]

*Corresponding author.
Email: dr.habibissaleh@gmail.com (H. Saleh), ishak_h@ukm.my (I. Hashim)

 ©2016 Global Science Press

https://doi.org/10.4208/aamm.2013.m419 Published online by Cambridge University Press

numerically investigated the effect of the magnetic field inside a rectangular enclosure and found that a circulating flow is formed with a relatively weak magnetic field and the rate of convective heat transfer is decreased when the magnetic field strength increases. [2] showed that the convection modes inside the enclosure strongly depend on both the strength and orientation of the magnetic field. [17] concluded that the magnetic field considerably decreases the average Nusselt number. [1] showed the suppression effect of the magnetic field on convection currents and heat transfer is more significant for low inclination angles of the enclosure and high Grashof numbers. For the similar configuration, [16] found that the Nusselt number increases up to about inclination angle 45° and then decrease as the angle increases. [15] applied steady and rotating magnetic fields to control the heat and mass transfer and the temperature fluctuations within the melt. Surprisingly, the rotating magnetic field was found very effective to stabilize the buoyant flow.

The effect of enclosure rotation on heat transfer is particularly very important concerning the flow of liquid metals inside enclosure, which is the standard material for manufacture of single wafer crystals in the semiconductor industry. [5] firstly studied the thermally driven flows in a rotating enclosure by using numerical technique. They found that the cells orientation change with increasing the rotation speeds. The fluid flow and heat transfer characteristics of a rotating square enclosure were studied experimentally and numerically by [7]. They concluded that the Coriolis force arising from rotation may have a remarkable influence on heat transfer when compared with non-rotating results and a correlation of Nusselt number as function of Taylor and Rayleigh number were built. [13] and [11,12] studied a differentially heated rotating cubic enclosure. Significant flow modification was obtained when the rotational Rayleigh number greater than the Rayleigh number or the Taylor number greater than the Rayleigh number. A significant increasing or decreasing in heat transfer in a rotating and differentially heated square enclosure could be achieved due to rotational effects as reported by [3] and [4]. [10] studied numerically the rectangular enclosure with discrete heat sources. They found that rotation results in imbalance of clockwise and counterclockwise circulations, increases heat transfer in the worst stage, reduces the oscillation of Nusselt number and improves or reduces mean performance in each cycle. The effects of body forces in a rotating and differentially heated enclosure is considered by [19]. The centrifugal force effect on heat transfer was found to be negligible. Recently, [14] found that the inertial and non-inertial results match well only for low rotational speeds of the enclosure.

The previous studies of the thermally driven flows in the presence of a magnetic field in a square enclosures have dealt with stationary enclosure. The present study considers thermally driven flows in the presence of a magnetic field of an arbitrary direction with rotating enclosure. The effects of the strength and orientation of the magnetic field and the rotational speeds on characteristics of convective flow and heat transfer performance are considered. For example, by precisely controlling the flow stability using a magnetic field, it is possible to extract a large single-crystal from the melt in the crystal growth process.

https://doi.org/10.4208/aamm.2013.m419 Published online by Cambridge University Press

2 Mathematical formulation

A schematic diagram of a square enclosure of side ℓ executes a steady uniform counter–clockwise rotation about its longitudinal axis as shown in Fig. 1, with the geometric layout and the Cartesian coordinates (x,y) rotating with the enclosure. The surface at $y=\ell/2$ has constant hot temperature (T_h) and the surface at $y=-\ell/2$ has a constant cold temperature (T_c). The temperatures along the lateral wall are assumed to be linearly distributed between T_h and T_c, i.e.,$(T_h+T_c)/2+(T_h-T_c)y/\ell$ to consider conjugate heat transfer in the lateral wall of the experiments. The φ shown in the Fig. 1 is defined as an angular position.

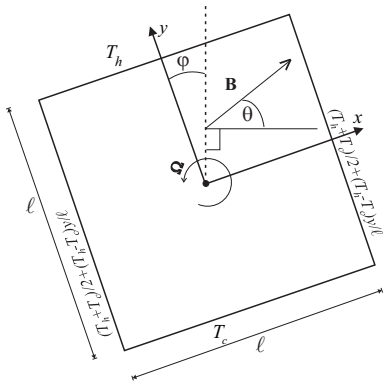


Figure 1: Schematic representation of the model.

The fluid is permeated by a uniform inclined magnetic field B_0. The magnetic field orientation is fixed during enclosure rotation. The magnetic Reynolds number is assumed to be small so that the induced magnetic field produced by the motion of the electrically conducting fluid is negligible compared to the applied magnetic field B_0. The fluid is Newtonian and the flow is laminar and incompressible. The density variation of the fluid follows Boussinesq's assumption and changes with temperature only. The terms representing the thermal and rotational buoyancies and Coriolis force are, respectively, equal to $\rho_0\mathbf{g}\beta(T-T_c)$, $-\rho_0\mathbf{g}\beta(T-T_c)\mathbf{\Omega}\times(\mathbf{\Omega}\times\mathbf{r})$ and $-2\rho_0[1-\beta(T-T_c)]\cdot\mathbf{\Omega}\times\mathbf{V}$. The continuity, momentum and energy equations can be described as follows:

$$\frac{\partial u}{\partial x}+\frac{\partial v}{\partial y}=0, \tag{2.1a}$$

$$\frac{\partial u}{\partial t}+u\frac{\partial u}{\partial x}+v\frac{\partial u}{\partial y}=-\frac{1}{\rho_0}\frac{\partial P_m}{\partial x}+\nu\left(\frac{\partial^2 u}{\partial x^2}+\frac{\partial^2 u}{\partial y^2}\right)+2\Omega v-2\Omega v\beta(T-T_c)-\Omega^2 x\beta(T-T_c)$$
$$+g\beta(T-T_c)\sin\Omega t+\frac{\sigma B_0^2}{\rho_0}(v\sin\theta\cos\theta-u\sin^2\theta), \tag{2.1b}$$

$$\frac{\partial v}{\partial t}+u\frac{\partial v}{\partial x}+v\frac{\partial v}{\partial y}=-\frac{1}{\rho_0}\frac{\partial P_m}{\partial y}+\nu\left(\frac{\partial^2 v}{\partial x^2}+\frac{\partial^2 v}{\partial y^2}\right)-2\Omega u+2\Omega u\beta(T-T_c)-\Omega^2 y\beta(T-T_c)$$

https://doi.org/10.4208/aamm.2013.m419 Published online by Cambridge University Press

$$+g\beta(T-T_c)\cos\Omega t+\frac{\sigma B_0^2}{\rho_0}(u\sin\theta\cos\theta-v\cos^2\theta), \tag{2.1c}$$

$$\frac{\partial T}{\partial t}+u\frac{\partial T}{\partial x}+v\frac{\partial T}{\partial y}=\alpha\left(\frac{\partial^2 T}{\partial x^2}+\frac{\partial^2 T}{\partial y^2}\right), \tag{2.1d}$$

where P_m is the motion pressure defined as:

$$P_m=p-\frac{1}{2}\rho_0\Omega^2x^2-\frac{1}{2}\rho_0\Omega^2y^2+\rho_0gx\sin(\Omega t)+\rho_0gy\cos(\Omega t). \tag{2.2}$$

Hence,

$$-\frac{\partial P_m}{\partial x}=-\frac{\partial p}{\partial x}+\rho_0\Omega^2x-\rho_0g\sin(\Omega t), \tag{2.3a}$$

$$-\frac{\partial P_m}{\partial y}=-\frac{\partial p}{\partial y}+\rho_0\Omega^2y-\rho_0g\cos(\Omega t). \tag{2.3b}$$

The governing equations (2.1a)-(2.1d) can be converted to nondimensional forms using the following nondimensional parameters:

$$X=\frac{x}{\ell},\qquad Y=\frac{y}{\ell},\qquad \tau=\frac{t\alpha}{\ell^2},\qquad U=\frac{u\ell}{\alpha}, \tag{2.4a}$$

$$V=\frac{v\ell}{\alpha},\qquad \Theta=\frac{T-T_c}{T_h-T_c},\qquad Pr=\frac{\nu}{\alpha},\qquad Ra=\frac{g\beta\left(T_h-T_c\right)\ell^3}{\nu\alpha}, \tag{2.4b}$$

$$P=\frac{P_m\ell^2}{\rho\alpha^2},\qquad Ra_\omega=\frac{\beta\Omega^2\left(T_h-T_c\right)\ell^4}{\nu\alpha},\qquad Ta=\frac{4\Omega^2\ell^4}{\nu^2},\qquad Ha=B_0\ell\sqrt{\frac{\sigma}{\rho_0\nu}}. \tag{2.4c}$$

The Coriolis buoyancy force is neglected, because $|\beta(T-T_c)|\ll 1$ in the present studies. The nondimensional continuity, momentum and energy equations are written as follows:

$$\frac{\partial U}{\partial X}+\frac{\partial V}{\partial Y}=0, \tag{2.5a}$$

$$\frac{\partial U}{\partial \tau}+U\frac{\partial U}{\partial X}+V\frac{\partial U}{\partial Y}=-\frac{\partial P}{\partial X}+Pr\left(\frac{\partial^2 U}{\partial X^2}+\frac{\partial^2 U}{\partial Y^2}\right)+\underbrace{Ta^{0.5}PrV}_{\text{Coriolis force term}}-\underbrace{Ra_\omega PrX\Theta}_{\text{Centrifugal force term}}$$
$$+\underbrace{RaPr\Theta\sin 0.5Ta^{0.5}Pr\tau}_{\text{Buoyancy force term}}+Ha^2Pr(V\sin\theta\cos\theta-U\sin^2\theta), \tag{2.5b}$$

$$\frac{\partial V}{\partial \tau}+U\frac{\partial V}{\partial X}+V\frac{\partial V}{\partial Y}=-\frac{\partial P}{\partial Y}+Pr\left(\frac{\partial^2 V}{\partial X^2}+\frac{\partial^2 V}{\partial Y^2}\right)-\underbrace{Ta^{0.5}PrU}_{\text{Coriolis force term}}-\underbrace{Ra_\omega PrY\Theta}_{\text{Centrifugal force term}}$$
$$+\underbrace{RaPr\Theta\cos 0.5Ta^{0.5}Pr\tau}_{\text{Buoyancy force term}}+Ha^2Pr(U\sin\theta\cos\theta-V\cos^2\theta), \tag{2.5c}$$

$$\frac{\partial \Theta}{\partial \tau}+U\frac{\partial \Theta}{\partial X}+V\frac{\partial \Theta}{\partial Y}=\frac{\partial^2 \Theta}{\partial X^2}+\frac{\partial^2 \Theta}{\partial Y^2}. \tag{2.5d}$$

https://doi.org/10.4208/aamm.2013.m419 Published online by Cambridge University Press

$U=V=0$ on the walls and the boundary conditions for the non-dimensional temperatures are:

$$\Theta = Y+0.5 \quad \text{at} \quad X=-0.5, \tag{2.6a}$$
$$\Theta = Y+0.5 \quad \text{at} \quad X=0.5, \tag{2.6b}$$
$$\Theta = 0 \quad \text{at} \quad Y=-0.5, \tag{2.6c}$$
$$\Theta = 1 \quad \text{at} \quad Y=0.5. \tag{2.6d}$$

The non-dimensional governing equations contain three independent dimensionless parameters, namely, Prandtl number, Rayleigh number and Taylor number. In addition, rotational Rayleigh number reflects the effect of centrifugal buoyancy force, but it depends on the other dimensionless parameters too [19].

The fluid motion is displayed using the stream function Ψ obtained from velocity components U and V. The relationships between the stream function and the velocity components are: $U=\partial\Psi/\partial Y$ and $V=-\partial\Psi/\partial X$, which yield a single equation,

$$\frac{\partial^2\Psi}{\partial X^2}+\frac{\partial^2\Psi}{\partial Y^2}=\frac{\partial U}{\partial Y}-\frac{\partial V}{\partial X}, \tag{2.7}$$

where $\Psi=0$ at all walls of the enclosure. The physical quantities of interest in this problem are the average Nusselt number, representation of the average heat transfer rate on the heated or cooled plates that defined by:

$$\overline{Nu}=\int_{-0.5}^{0.5}\frac{\partial\Theta}{\partial Y}dX. \tag{2.8}$$

The time-integrated of the average heat transfer rate in one cycle is:

$$\overline{\overline{Nu}}=\frac{1}{\tau_p}\int_0^{\tau_p}\overline{Nu}d\tau. \tag{2.9}$$

3 Numerical method and validation

Staggered grid arrangement together with the Marker and Cell (MAC) method [8] are adopted to solve the governing equations (2.5a)-(2.5d) subject to the boundary conditions (2.6a)-(2.6d). Due to lack of boundary conditions for pressure, the use of the staggered grid and MAC formulation provide an advantage. That is, one may locate the secondary grid along the boundaries of the domain where only specification of velocity boundary conditions is required but not of the pressure. The fictitious values of velocity outside the domain are obtained by extrapolation of the interior points as given by [9]. A second-order central difference approximation is used for the space discretization and a first-order approximation is used for temporal derivative. The solution of the Poisson pressure equation is obtained by applying an iterative Gaussian-SOR method. The velocities are then computed by the projection method.

https://doi.org/10.4208/aamm.2013.m419 Published online by Cambridge University Press

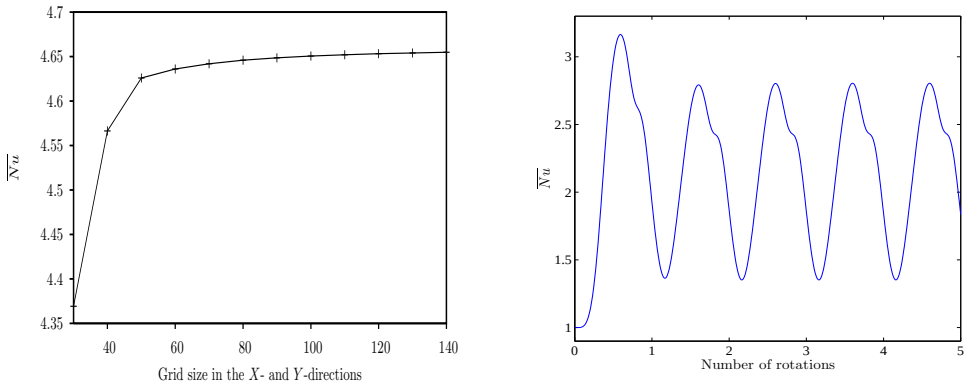


Figure 2: (a) Grid independency study: $\overline{Nu_f}$ versus number of grid points, (b) Typical computation process for present periodic oscillation problem.

In this study, the convergence criterion for the Poisson equation is set as $\epsilon = 10^{-5}$ and the time stepping is chosen, $\Delta\tau = \lambda(1/4)(\Delta X)^2 Pr$ to meet stability criteria, where λ is the safety factor with the value between 0 and 1. Uniform grid distribution is used for the whole enclosure. The effect of grid resolution was examined in order to select the appropriate grid density as demonstrated in Fig. 2(a) for $Ha = 30$, $\theta = 0^\circ$, $Ta = 8.9\times10^4$, $Ra = 1.2\times10^5$ at $\varphi = 5\pi/4$. The results indicate that an 120×120 mesh can be used in the final computations. A typical computation process for the present periodic oscillation problem for Ha=30, θ=0°, Ta=8.9×10^4, Ra=1.2×10^5 is shown in Fig. 2(b) where, the final periodic oscillation of the $\overline{Nu}$ is obtained after two rotations. Therefore, all computations in this work were carried out beyond two rotations. As a validation, our results for the isotherms compare well with that [19] and the streamlines compare equivalent with that obtained by [7] for a special case, Ha=0, Ra=1.2×10^5, Ta=8.9×10^4 as shown in Fig. 3(a) and (b), respectively. Small deviation in the cells circulation shape may be credited to coarse, 36×36 uniform grid used by [7]. [19] applied the finite volume method and [7] applied the control volume finite difference method.

4 Results and discussion

The analysis in the undergoing numerical investigation is performed in the following range of the associated dimensionless groups: the Hartmann number, $0 \le Ha \le 70$, the inclination angle of the magnetic field, $0^\circ \le \theta \le 90^\circ$ and the Taylor number, $8.9\times10^4 \le Ta \le 1.1\times10^6$. Other parameters are $T_h = 282$K, $T_c = 273$K, $\ell = 0.0508$m, $Pr = 0.7$, $Ra = 1.2\times10^5$, $\Omega = 8.5$ to 30rpm and $Ra_\omega = 496$ to 6183. The rotational Rayleigh number, Ra_ω, was not discussed except to specify it explicitly. This is due to the Ra_ω not being an independent parameter but depending on Pr and Ra as well as Ta. We note that in the present research the Coriolis force is stronger than the centrifugal force. The flow and thermal fields inside

https://doi.org/10.4208/aamm.2013.m419 Published online by Cambridge University Press

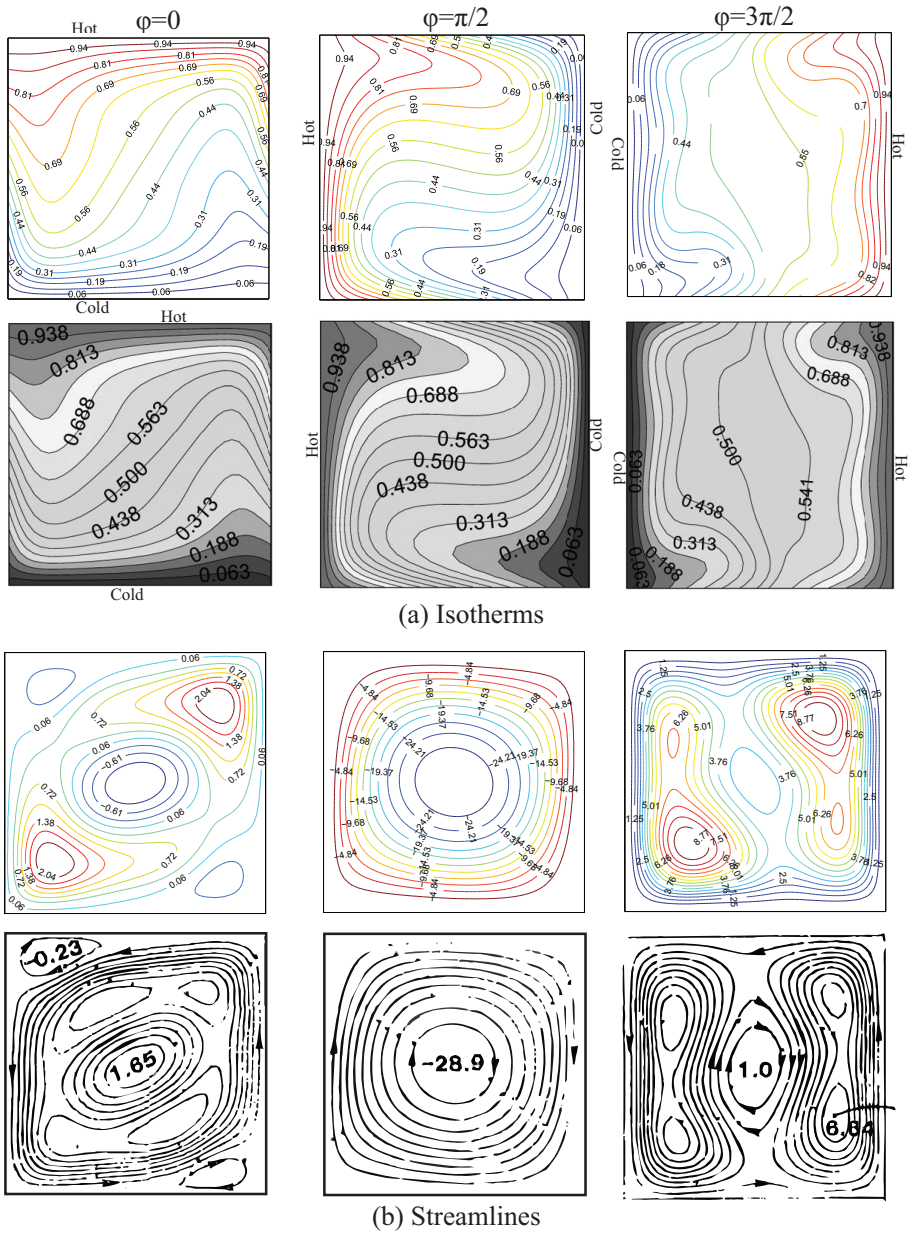


Figure 3: Comparison of computed (a) isotherms of present work with [19] and (b) streamlines of present work with [7] for a special case, $Ha=0$, $Ra=1.2\times10^5$, $Ta=8.9\times10^4$.

the enclosure during rotation will be shown in Fig. 4 and Fig. 5. The average Nusselt number over one period will be presented in Fig. 6. Finally, plots of the global quantity average Nusselt number over one cycle will be displayed in Fig. 7 and Fig. 8.

Figs. 4(a)-(h) presents the effects of rotation on the flow field for different magnetic

https://doi.org/10.4208/aamm.2013.m419 Published online by Cambridge University Press

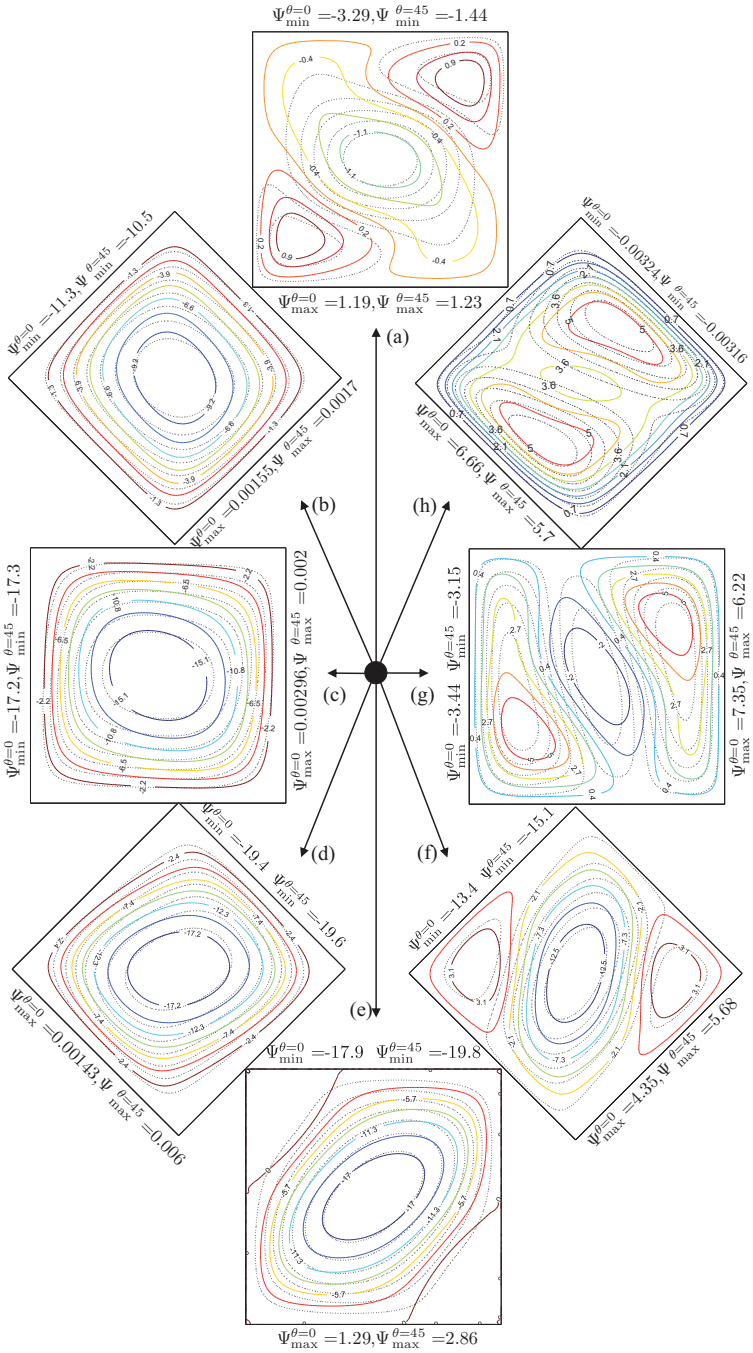


Figure 4: Streamlines [$\theta=0^\circ$ (solid lines) and $\theta=45^\circ$ (dashed lines)] evolution during one period for $Ha=20$ and $Ta=8.9\times10^4$ when (a) $\varphi=0$, (b) $\varphi=\pi/4$, (c) $\varphi=\pi/2$, (d) $\varphi=3\pi/4$, (e) $\varphi=\pi$, (f) $\varphi=5\pi/4$, (g) $\varphi=3\pi/2$, (h) $\varphi=7\pi/4$.

https://doi.org/10.4208/aamm.2013.m419 Published online by Cambridge University Press

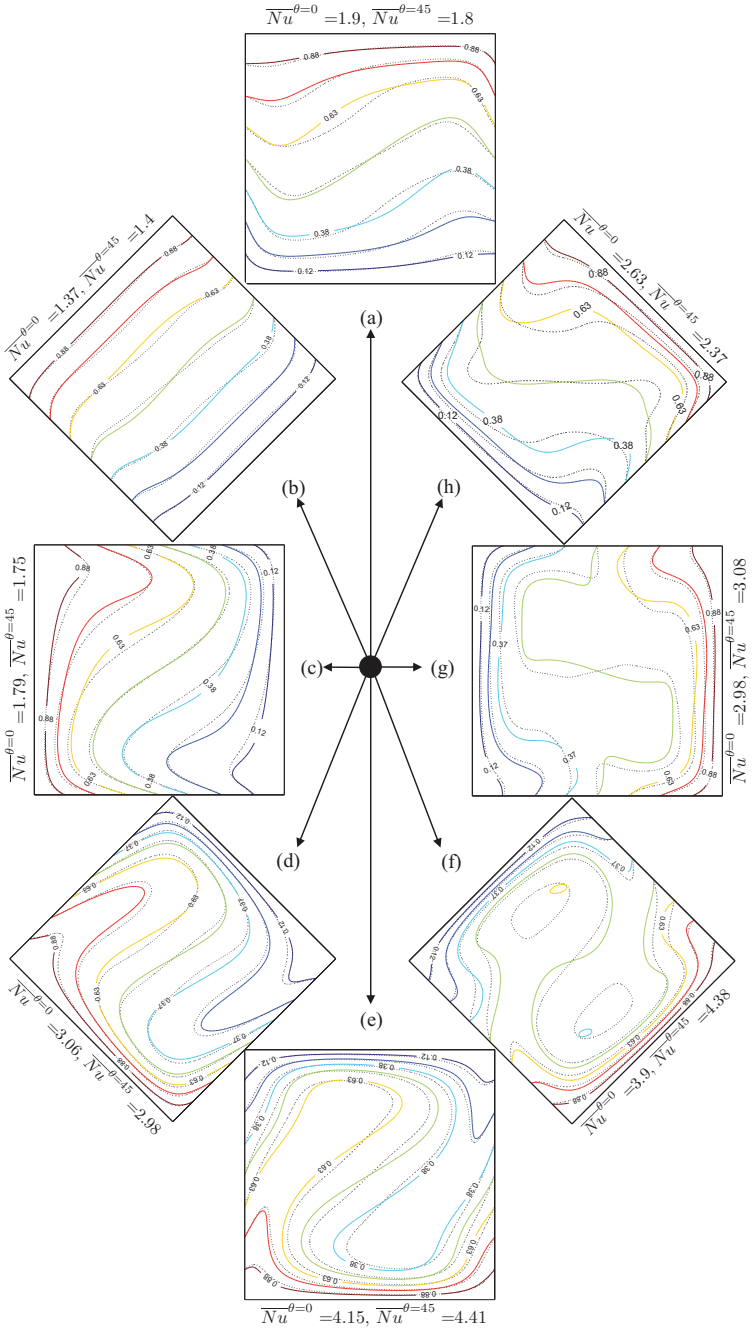


Figure 5: Isotherms [$\theta=0^\circ$ (solid lines) and $\theta=45^\circ$ (dashed lines)] evolution during one period for $Ha=20$ and $Ta=8.9\times10^4$ when (a) $\varphi=0$, (b) $\varphi=\pi/4$, (c) $\varphi=\pi/2$, (d) $\varphi=3\pi/4$, (e) $\varphi=\pi$, (f) $\varphi=5\pi/4$, (g) $\varphi=3\pi/2$, (h) $\varphi=7\pi/4$.

https://doi.org/10.4208/aamm.2013.m419 Published online by Cambridge University Press

field direction at $Ha=20$ and $Ta=8.9\times10^4$. There are two basic flow structures inside the enclosure, clockwise (negative sign) and counterclockwise (positive sign) circulations. It relies on the heated position and the inertial forces. Starting from $\varphi=\pi/4$ where the heated wall is above the cold wall, one observes a mono eddy circulation inside the enclosure. The circulation is in a clockwise direction due to the thermally driven force. This flow persists up to $\varphi=3\pi/4$. At the Bénard convection problem, $\varphi=\pi$, the positive flow is detected, see $\Psi_{\max}$ values. At $\varphi=5\pi/4$, subplot (f), the effect of buoyancy force is now to induce a positive flow circulation, but the flow inertia from the negative flow circulation still prevail. The both flows compete each other, where a clockwise cell in the middle and two smaller cells in the corners rotating in the positive direction where the effect of the Coriolis force is small. With increasing the orientation angle, the counterclockwise cells in the corner get stronger and bigger, push the clockwise cell in the center enclosure. Finally at $\varphi=7\pi/4$, subplot (h), the clockwise cell shrink and disappear or the transition from negative to positive flow is done. The positive flows get slightly weaker. This due to the Coriolis force now outward and unwavering flow circulation. The negative flow return back at $\varphi=2\pi$ or 0 rad. Note that this sequence repeats itself, the fully negative flow, transition and fully positive flow. It is observed that during half rotation, subplots (g)-(b), the strength of the flow circulation of the inclined Lorentz force is weaker than the horizontal Lorentz force direction, as indicated from $|\Psi_{\min}|$ and $\Psi_{\max}$ values. The different result was obtained during the other half rotation.

Figs. 5(a)-(h) present the effects of rotation on the temperature field for different magnetic field direction at $Ha=20$ and $Ta=8.9\times10^4$. The hot or cold walls positions change according to the angular phase shift. Starting from $\varphi=\pi/4$ where the hot wall above the cold wall. When the wall temperature rise, it is followed by increasing the fluid temperature adjoining the wall which creates a clockwise motion as shown in the previous figure. The isotherms exhibit almost straight lines that indicates the weak convection heat transfer. The convection strength is strengthen by increasing the rotation angle as represented by the average Nusselt number value. Increasing the angle further enhance the $\overline{Nu}$. At $\varphi=5\pi/4$, subplot (f), the $\overline{Nu}$ is suppressed by the stabilization effect of the Coriolis force. This point can be understood from the existence negative and positive flow circulation in the streamlines. The $\overline{Nu}$ value of the inclined Lorentz force is smaller than the horizontal Lorentz force direction as shown in subplots (a)–(d), unparallel with the strength of the flow circulation as discussed before.

Fig. 6(a) depicts the variation of the average Nusselt number, $\overline{Nu}$, over one period for different Hartmann at $\theta=45^\circ$, Fig. 6(b) depicts arbitrary magnetic field direction at $Ha=20$ and $Ta=8.9\times10^4$ and Fig. 6(c) depicts various rotational speed (Taylor numbers) at $Ha=20$ and $\theta=45^\circ$. It observed that in general a higher Ha lead to greater suppression of the $\overline{Nu}$ at any angular location as shown in Fig. 6(a). At very high magnetic field, $Ha=70$, the average Nusselt number remains constant by shifting the angular location. The heat transfer is dominated by the conduction mode. It observed from Fig. 6(b) that variation of the magnetic direction gives significant effect from $\varphi=7\pi/8$ to $\varphi=2\pi$. During rotation, increasing the Taylor number stabilizes the $\overline{Nu}$ as presented in Fig. 6(c). It is also observed

https://doi.org/10.4208/aamm.2013.m419 Published online by Cambridge University Press

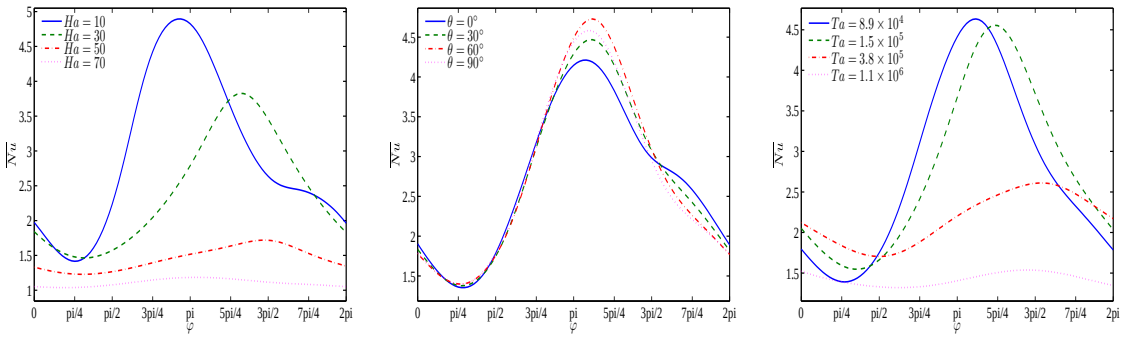


Figure 6: Average Nusselt number against φ for the different values of Ha (a), θ (b) and Ta (c).

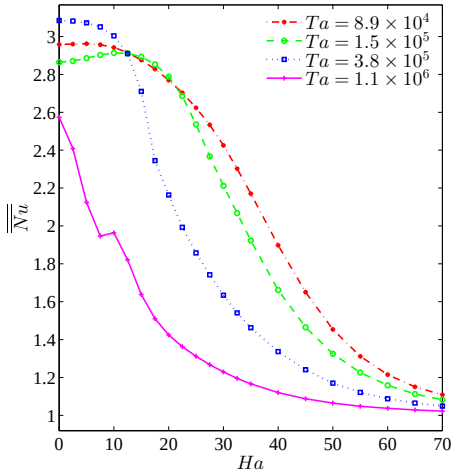


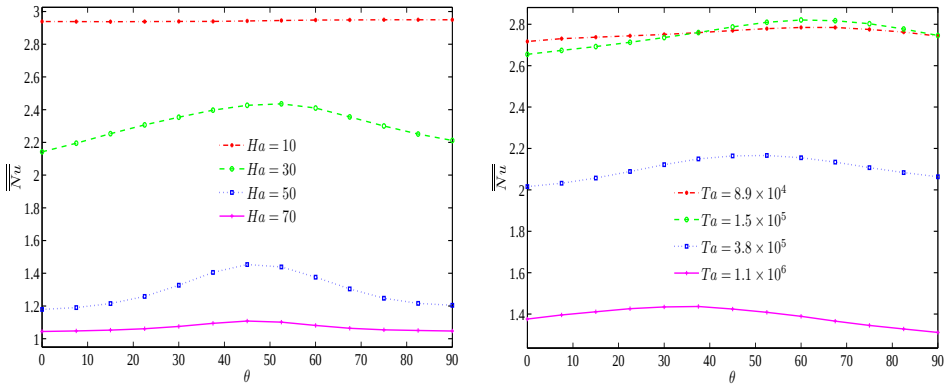
Figure 7: Global quantity average Nusselt number for various values of Ta against Ha.

that angular locations of the local maximum and minimum of the Nusselt number change by varying the magnetic field strength or the rotational speed. However, the angular locations of the local maximum and minimum are fixed by varying the magnetic field orientation.

Fig. 7 shows the the global quantity average Nusselt number for different Taylor numbers against the Hartmann number at $\theta = 45^\circ$. The global heat transfer performance decreases nonlinearly by increasing the Ha. This due to the flow circulation is progressively inhibited by the retarding effect of the electromagnetic body force. As a result of this phenomenon, the convection strength are much lower at stronger Ha. At relative weak magnetic field, $Ha < 20$, no consistent tendency effect of the rotational speed to the $\overline{\overline{Nu}}$. However at $Ha > 20$, a higher rotational speed gives a lower $\overline{\overline{Nu}}$ at the fixed Ha.

Figs. 8(a) and (b) presents the the global quantity average Nusselt number for differ-

https://doi.org/10.4208/aamm.2013.m419 Published online by Cambridge University Press



(a) (b)

Figure 8: Global quantity average Nusselt number for various values of Ha (a) and Ta (b) against θ.

ent Hartmann numbers at $Ta = 8.9 \times 10^4$ and various rotational speeds at $Ha = 20$ against the direction of the magnetic field. It observed from Fig. 8(a), a stronger Ha decreases the $\overline{\overline{Nu}}$ at all magnetic field direction. The $\overline{\overline{Nu}}$ profiles exhibits almost symmetry shape to axis $\theta = 45°$. This result also reveals that $\theta = 45°$ has less effect to the the global quantity average Nusselt number. It observed from Fig. 8(b) that horizontal or vertical direction of the magnetic field was most effective in reducing the global quantity of the average Nusselt number for the considered rotational speed. A higher rotational speed gives lower $\overline{\overline{Nu}}$ at all θ except at relative slow rotational speed.

5 Conclusions

Detailed computational results for flow fields and the thermal performance of the rotating enclosure in the presence of an inclined magnetic field have been presented in the graphical forms. The main conclusions of the present analysis are as follows:

1. Positions of local maximum and minimum heat transfer rate change by varying the magnetic field strength or the rotational speed, but the positions are fixed by varying the magnetic field orientation.

2. Increasing the Lorentz force or rotational speed stabilizes the flow and heat transfer oscillation. A sufficiently large Lorentz force neutralizes the effect of buoyancy, inertial and Coriolis forces.

3. Horizontal or vertical direction of the magnetic field was most effective in reducing the global heat transfer.

https://doi.org/10.4208/aamm.2013.m419 Published online by Cambridge University Press

Nomenclature

B_0	magnitude of the magnetic filed (T)
Cp	specific heat capacity (J/kgK)
g	gravitational acceleration (m/s^2)
Ha	Hartmann number
k	thermal conductivity (Wm^{-1}K^{-1})
ℓ	width and height of enclosure (m)
Nu	Nusselt number
Ra	Rayleigh number
Ra_ω	rotational Rayleigh number
Ta	Taylor number
T	temperature (K)
u, v	velocity components in the x- and y-directions (m/s)
x, y & X, Y	space coordinates (m) & dimensionless space coordinates
α	thermal diffusivity (m^2/s)
β	thermal expansion coefficient (1/K)
θ	inclination angle of the magnetic field (deg)
τ	dimensionless time
τ_p	dimensionless time for one rotation
Θ	dimensionless temperature
Ω	magnitude of angular rotation rate (rpm, rad/s)
ρ	density (kg/m^3)
Ψ	dimensionless stream function
φ	angular position of enclosure (rad)
μ	dynamic viscosity (Ns/m^2)
c	cold
h	hot

Acknowledgments

The work was supported partially by the Malaysian Ministry of Education through the Fundamental Research Grant Scheme No. FRGS/1/2014/SG04/UKM/01/1.

References

[1] N. M. Al-Najem, K. M. Khanafer and M. M. El-Refaee, *Numerical study of laminar natural convection in tilted enclosure with transverse magnetic field,* Int. J. Numer. Meth. Heat Fluid Flow, 8 (1998), pp. 651–672.

[2] S. Alchaar, P. Vasseur and E. Bilgen, *Natural convection heat transfer in a rectangular enclosure with a transverse magnetic field,* J. Heat Transfer, 117 (1995), pp. 668–673.

https://doi.org/10.4208/aamm.2013.m419 Published online by Cambridge University Press

[3] M. F. BAIG AND A. MASOOD, *Natural convection in a two-dimensional differentially heated square enclosure undergoing rotation,* Numer. Heat Transfer Part A, 40 (2001), pp. 181–202.
[4] M. F. BAIG AND M. ZUNAID, *Numerical simulation of liquid metals in differentially heated enclosure undergoing orthogonal rotation,* Int. J. Heat Mass Transfer, 49 (2006), pp. 3500–3513.
[5] K. BUHLER AND H. OERTEL, *Thermal cellular convection in rotating rectangular boxes,* J. Fluid Mech., 114 (1982), pp. 261–282.
[6] J. P. GARANDET, T. ALBUSSOIERE AND R. MOREAU, *Buoyancy driven convection in a rectangular enclosure with a transverse magnetic field,* Int. J. Heat Mass Transfer, 35 (1992), pp. 741–748.
[7] F. J. HAMADY, J. R. LLOYD, K. T. YANG AND H. Q. YANG, *A study of natural convection in a rotating enclosure,* J. Heat Transfer, 116 (1994), pp. 136–143.
[8] F. HARLOW AND J. E. WELCH, *Numerical calculation of time-dependent viscous incompressible flow of fluid with a free surface,* Phys. Fluids, 8 (1965), pp. 2182–2189.
[9] K. A. HOFFMANN AND S. T. CHIANG, Computational Fluid Dynamics Volume I, Engineering Education System, Kansas, 2000.
[10] L. F. JIN, S. K. W. TOU AND C. P. TSO, *Effects of rotation on natural convection cooling from three rows of heat sources in a rectangular cavity,* Int. J. Heat Mass Transfer, 48 (2005), pp. 3982–3994.
[11] Y. T. KER AND T. F. LIN, *A combined numerical and experimental study of air convection in a differentially heated rotating cubic cavity,* Int. J. Heat Mass Transfer, 39 (1996), pp. 3193–3210.
[12] Y. T. KER AND T. F. LIN, *Time-averaged and reverse transition in oscillatory air convection in a differentially heated rotating cubic cavity,* Int. J. Heat Mass Transfer, 40 (1997), pp. 3335–3349.
[13] T. L. LEE AND T. F. LIN, *Transient three-dimensional convection of air in a differentially heated rotating cubic cavity,* Int. J. Heat Mass Transfer, 39 (1996), pp. 1243–1255.
[14] J. C. MANDAL AND C. R. SONAWANE, *Simulation of flow inside differentially heated rotating cavity*, Int. J. Numer. Meth. Heat Fluid Flow, 23 (2013), pp. 23–54.
[15] R. MÖSSNER AND G. GERBETH, *Buoyant melt flows under the infuence of steady and rotating magnetic felds*, J. Crystal Growth, 197 (1999), pp. 341–354.
[16] M. PIRMOHAMMADI AND M. GHASSEMI, *Effect of magnetic field on convection heat transfer inside a tilted square enclosure*, Int. Commun. Heat Mass Transfer, 36 (2009), pp. 776–780.
[17] M. PIRMOHAMMADI, M. GHASSEMI AND G. A. SHEIKHZADEH, *Effect of a magnetic field on buoyancy-driven convection in differentially heated square cavity,* IEEE Transactions Magnetics, 45 (2009), pp. 407–411.
[18] N. RUDRAIAH, R.M. BARRON, M. VENKATACHALAPPA AND C. K. SUBBARAYA, *Effect of a magnetic field on free convection in a rectangular enclosure,* Int. J. Eng. Sci., 33 (1995), pp. 1075–1084.
[19] C. P. TSO, L. F. JIN AND S. K. W. TOU, *Numerical segregation of the effects of body forces in a rotating, differentially heated enclosure,* Numer. Heat Transfer Part A, 51 (2007), pp. 85–107.

https://doi.org/10.4208/aamm.2013.m419 Published online by Cambridge University Press